small bone chips (2 mm average diameter) using a bone mill. Radiometric analysis in a loading experiment revealed that the acetabular components had greater stability when large bone chips were used [20]. However, based on the Mohr-Coulomb failure criterion, both the angle of shearing resistance and the interlocking of the bone particles define the shear strength. Because the angle of shearing resistance depends on the distribution of particle size and because smaller particles fill the voids and interlock within the interparticulate spaces between larger particles, well-graded aggregates comprising a mixture of various-sized bone chips should have better mechanical characteristics compared with an ungraded mixture. Fosse et al. [8] reported that the bone aggregates with particles of uniform size have worse mechanical properties than those with a wider range of particle sizes. In our study, the mixture of different-sized bone chips did not markedly affect the stiffness properties of the bone aggregates. A possible reason for this difference relates to the different sizes of the bone particles. The bone mill used in our study cannot produce very small particles (less than 2 mm in diameter), and we used small-sized particles (3–4 mm in diameter) mixed with large-sized particles. Another possible explanation is that the ex vivo compaction device in our study loads more than 3,000 N of creep compression force and more than 4,700 N of impaction force, which crushes the trabecular structure of the bone chips. Small crushed bone fragments occupy the interparticulate spaces.

Recoil

In our study, recoil of the graft aggregates was 2.6–3.9% of the initial height of the compacted bone aggregates made by the ex vivo compaction device, and recoil did not correlate with the bone chip size. Previous studies showed that the impaction force, particle size, and fluid content influence recoil behavior significantly [11, 21]. Our ex vivo compaction device allows excess incompressible fluid exudation during use of the creep technique and crushes the trabecular structure of the bone particles during used of the creep and impaction technique, so that the particles lose their elasticity. In addition, small crushes of bone fragments and a mixture of various sizes of the bone chips reduce the void space and interlock each bone particle within the aggregates, reducing the recoil. Our micro-CT data visualized the collapsed trabeculae and the bone particles riding over each other.

Cement penetration

Closer packing increases the interparticulate contacts and the shear strength of the bone aggregates [7, 21]. However, well-compacted, well-graded bone aggregates can limit cement penetration into the interparticulate spaces. Because the bone cement creates a solid layer of bone at the graft-cement interface, greatly increasing the constant of the interlocking of the bone particles in the Mohr-Coulomb failure criterion contributes to the mechanical characteristics of the bone aggregates. Larger bone grafts should provide better penetration of the bone cement within the graft layer. Our data indicate that the maximal depth of cement penetration into the bone aggregates varies in relation to the proportion of large bone chips. This is because of the larger pores between the bone chips, even when a well-compacted bone aggregate can be produced using the ex vivo compaction device. Thus, bone aggregates made up with large-sized bone chips may produce better initial stability of the acetabular component.

Osteoconductivity

Several previous studies showed new bone formation onto the surfaces of the allograft bone chips and that regeneration and remodeling continue gradually for several years. Regeneration, remodeling, and a lasting bond between the graft and the host are prerequisites for the long-term success of impaction bone grafting. Pore size and interconnectivity are among the most important factors for osteoconduction by porous biomaterials [16, 18, 19, 29]. The optimal pore size for bone growth is generally considered to be 100–400 μm. We had some concerns that a well-compacted, well-graded mixture might hamper osteoconduction into the graft by filling up the interparticulate spaces. However, micro-CT analysis revealed that the grafts had adequate porous structure for osteoconduction and potential to encourage the bone graft healing process, which provides scaffolding for the ingrowth of vessels and osteoprogenitor cells to induce graft incorporation by the host [18, 19]. By contrast, bone aggregates comprising only large-sized bone chips tend to possess more pores, which may be too large to optimize bone growth, although few studies have reported on the adverse effects of large pores on osteoconduction [18, 19]. Thus, the bone aggregates produced with small-sized bone chips may provide superior osteoconductivity. Our data suggest that the graft layer on the host bone should comprise small-sized bone particles to facilitate bone ingrowth and that the layer on the implant side should be produced with large-sized bone particles to maximize cement penetration. Further studies are needed to confirm this hypothesis.

Clinical cases

In our clinical practice, we performed acetabular reconstruction by impaction bone grafting using the ex vivo compaction device in eight patients. Because most

migration and subsidence of the implant occurred during the first 3 months after implantation, as reported previously [30], the short-term outcome of the patients in this study indicated that the procedure was successful. We note that, after removing the compacted bone aggregates from the ex vivo compaction device, further creep consolidation of the bone aggregate with an impaction phantom formed a layer of well-compacted, well-graded bone aggregates in the acetabular defect in vivo. We also maintained the pressure on the graft bed to avoid possible recoil until the acetabular component was cemented. This procedure should contribute to the initial stiffness of the bone aggregates, leading to the initial stability of the acetabular component. We have applied this technique to acetabular reconstruction in patients, and no implant has exhibited any subsidence during a short-term follow-up period. Further clinical studies are required to determine the mid- and long-term outcomes of this technique.

In conclusion, the ex vivo compaction device produces well-compacted, well-graded allograft bone aggregates that possess adequate mechanical properties and putative osteoconductivity. Progressive compaction of layers of aggregates, comprising smaller sized chips at the host bone side and larger sized chips at the component side, may have the advantages of initial stability of the acetabular component and biological response of the grafted aggregates in acetabular reconstruction of revision THA.

Conflict of interest None of the authors of this manuscript has received any type of support, benefits, or funding from any commercial party related directly or indirectly to the subject of this article.

References

1. Gie GA, Linder L, Ling RS, Simon JP, Slooff TJ, Timperley AJ. Impacted cancellous allografts and cement for revision total hip arthroplasty. J Bone Joint Surg Br. 1993;75(1):14–21.
2. Slooff TJ, Huiskes R, van Horn J, Lemmens AJ. Bone grafting in total hip replacement for acetabular protrusion. Acta Orthop Scand. 1984;55(6):593–6.
3. Comba F, Buttaro M, Pusso R, Piccaluga F. Acetabular reconstruction with impacted bone allografts and cemented acetabular components: a 2- to 13-year follow-up study of 142 aseptic revisions. J Bone Joint Surg Br. 2006;88(7):865–9.
4. Iwase T, Masui T, Torii Y, Kouyama A. Impaction bone grafting for acetabular reconstruction: mean 5.5-year results in Japanese patients. Arch Orthop Trauma Surg 2009 (in press).
5. Schreurs BW, Bolder SB, Gardeniers JW, Verdonschot N, Slooff TJ, Veth RP. Acetabular revision with impacted morsellised cancellous bone grafting and a cemented cup. A 15- to 20-year follow-up. J Bone Joint Surg Br. 2004;86(4):492–7.
6. van Haaren EH, Heyligers IC, Alexander FG, Wuisman PI. High rate of failure of impaction grafting in large acetabular defects. J Bone Joint Surg Br. 2007;89(3):296–300.
7. Brewster NT, Gillespie WJ, Howie CR, Madabhushi SP, Usmani AS, Fairbairn DR. Mechanical considerations in impaction bone grafting. J Bone Joint Surg Br. 1999;81(1):118–24.
8. Fosse L, Ronningen H, Benum P, Lydersen S, Sandven RB. Factors affecting stiffness properties in impacted morsellized bone used in revision hip surgery: an experimental in vitro study. J Biomed Mater Res A. 2006;78(2):423–31.
9. Fosse L, Ronningen H, Lund-Larsen J, Benum P, Grande L. Impacted bone stiffness measured during construction of morsellised bone samples. J Biomech. 2004;37(11):1757–66.
10. Ornstein E, Franzen H, Johnsson R, Stefansdottir A, Sundberg M, Tagil M. Five-year follow-up of socket movements and loosening after revision with impacted morselized allograft bone and cement: a radiostereometric and radiographic analysis. J Arthroplasty. 2006;21(7):975–84.
11. Ullmark G, Nilsson O. Impacted corticocancellous allografts: recoil and strength. J Arthroplasty. 1999;14(8):1019–23.
12. Ornstein E, Atroshi I, Franzen H, Johnsson R, Sandquist P, Sundberg M. Early complications after one hundred and forty-four consecutive hip revisions with impacted morselized allograft bone and cement. J Bone Joint Surg Am. 2002;84-A(8):1323–8.
13. Tanabe Y, Wakui T, Kobayashi A, Ohashi H, Kadoya Y, Yamano Y. Determination of mechanical properties of impacted human morsellized cancellous allografts for revision joint arthroplasty. J Mater Sci Mater Med. 1999;10(12):755–60.
14. D'Antonio JA, Capello WN, Borden LS, Bargar WL, Bierbaum BF, Boettcher WG, Steinberg ME, Stulberg SD, Wedge JH. Classification and management of acetabular abnormalities in total hip arthroplasty. Clin Orthop Relat Res. 1989;243:126–37.
15. Albert C, Masri B, Duncan C, Oxland T, Fernlund G. Impaction allografting—the effect of impaction force and alternative compaction methods on the mechanical characteristics of the graft. J Biomed Mater Res B Appl Biomater. 2008;87(2):395–405.
16. Otsuki B, Takemoto M, Fujibayashi S, Neo M, Kokubo T, Nakamura T. Pore throat size and connectivity determine bone and tissue ingrowth into porous implants: three-dimensional micro-CT based structural analyses of porous bioactive titanium implants. Biomaterials. 2006;27(35):5892–900.
17. Merle d'Aubigné R, Postel M. Functional results of hip arthroplasty with acrylic prosthesis. J Bone Joint Surg Am. 1954;36:451–75.
18. Bobyn JD, Pilliar RM, Cameron HU, Weatherly GC. The optimum pore size for the fixation of porous-surfaced metal implants by the ingrowth of bone. Clin Orthop Relat Res. 1980;150:263–70.
19. Kujala S, Ryhanen J, Danilov A, Tuukkanen J. Effect of porosity on the osteointegration and bone ingrowth of a weight-bearing nickel-titanium bone graft substitute. Biomaterials. 2003;24(25):4691–7.
20. Arts JJ, Verdonschot N, Buma P, Schreurs BW. Larger bone graft size and washing of bone grafts prior to impaction enhances the initial stability of cemented cups: experiments using a synthetic acetabular model. Acta Orthop. 2006;77(2):227–33.
21. Dunlop DG, Brewster NT, Madabhushi SP, Usmani AS, Pankaj P, Howie CR. Techniques to improve the shear strength of impacted bone graft: the effect of particle size and washing of the graft. J Bone Joint Surg Am. 2003;85-A(4):639–46.
22. Voor MJ, White JE, Grieshaber JE, Malkani AL, Ullrich CR. Impacted morselized cancellous bone: mechanical effects of defatting and augmentation with fine hydroxyapatite particles. J Biomech. 2004;37(8):1233–9.
23. Craig RF. Craig's soil mechanics. 7th ed. New York: Spon Press; 2004.
24. Lunde KB, Kaehler N, Ronningen H, Fosse L. Pressure during compaction of morsellised bone gives an increase in stiffness: an in vitro study. J Biomech. 2008;41(1):231–4.
25. Ohman C, Baleani M, Perilli E, Dall'Ara E, Tassani S, Baruffaldi F, Viceconti M. Mechanical testing of cancellous bone from the femoral head: experimental errors due to off-axis measurements. J Biomech. 2007;40(11):2426–33.

26. Ahmed TA, Dare EV, Hincke M. Fibrin: a versatile scaffold for tissue engineering applications. Tissue Eng Part B Rev. 2008;14(2):199–215.
27. Bavadekar A, Cornu O, Godts B, Delloye C, Van Tomme J, Banse X. Stiffness and compactness of morselized grafts during impaction: an in vitro study with human femoral heads. Acta Orthop Scand. 2001;72(5):470–6.
28. Bolder SB, Schreurs BW, Verdonschot N, van Unen JM, Gardeniers JW, Slooff TJ. Particle size of bone graft and method of impaction affect initial stability of cemented cups: human cadaveric and synthetic pelvic specimen studies. Acta Orthop Scand. 2003;74(6):652–7.
29. Takemoto M, Fujibayashi S, Otsuki B, Matsushita T, Kokubo T, Nakamura T. 3-D anallysis of pore structure of porous biomaterials using micro focus X-ray computed tomography. Bioceramics. 2006;18:1095–8.
30. Ornstein E, Franzén H, Johnsson R, Sandquist P, Stefánsdóttir A, Sundberg M. Migration of the acetabular component after revision with impacted morselized allografts: a radiostereometric 2-year follow-up analysis of 21 cases. Acta Orthop Scand. 1999;70(4):338–42.

J Mater Sci: Mater Med (2011) 22:1803–1812
DOI 10.1007/s10856-011-4372-x

Nanostructured positively charged bioactive TiO_2 layer formed on Ti metal by NaOH, acid and heat treatments

Deepak K. Pattanayak · Seiji Yamaguchi · Tomiharu Matsushita · Tadashi Kokubo

Received: 15 April 2011 / Accepted: 4 June 2011 / Published online: 14 June 2011

Abstract Nanometer-scale roughness was generated on the surface of titanium (Ti) metal by NaOH treatment and remained after subsequent acid treatment with HCl, HNO_3 or H_2SO_4 solution, as long as the acid concentration was not high. It also remained after heat treatment. Sodium hydrogen titanate produced by NaOH treatment was transformed into hydrogen titanate after subsequent acid treatment as long as the acid concentration was not high. The hydrogen titanate was then transformed into titanium oxide (TiO_2) of anatase and rutile by heat treatment. Treated Ti metals exhibited high apatite-forming abilities in a simulated body fluid especially when the acid concentration was greater than 10 mM, irrespective of the type of acid solutions used. This high apatite-forming ability was maintained in humid environments for long periods. The high apatite-forming ability was attributed to the positive surface charge that formed on the TiO_2 layer and not to the surface roughness or a specific crystalline phase. This positively charged TiO_2 induced apatite formation by first selectively adsorbing negatively charged phosphate ions followed by positively charged calcium ions. Apatite formation is expected on the surfaces of such treated Ti metals after short periods, even in living systems. The bonding of metal to living bone is also expected to take place through this apatite layer.

D. K. Pattanayak (✉) · S. Yamaguchi · T. Matsushita · T. Kokubo
Department of Biomedical Sciences, College of Life and Health Sciences, Chubu University, 1200 Matsumoto-cho, Kasugai 487-8501, Japan
e-mail: deepak@isc.chubu.ac.jp; deepak_pattanayak@rediffmail.com

1 Introduction

Various surface treatment methods have been employed in an attempt to induce the bone-bonding property of titanium (Ti) metal and its alloys [1–14]. Of the treatment methods considered, the formation of sodium titanate on Ti metal by treating with both NaOH and heat has been shown to be effective for inducing apatite formation on Ti metal in the human body and causing Ti metal to bond to living bone through the apatite layer [15–18]. This method was applied to a porous Ti metal layer of an artificial hip joint, and the resulting bone bonding, i.e., a bioactive hip joint, has been clinically used in Japan since 2007 [19]. Apatite formation on NaOH- and heat-treated Ti metal in the living body was attributed to the negative surface charge of sodium titanate.

In contrast, it was recently shown that combining acid and heat treatment to form TiO_2 on Ti metal effectively induces apatite formation in the body environment and causes Ti metal to bond to living bone through the apatite layer [20]. The apatite formation in this case was attributed to the positive surface charge of TiO_2 [20].

Treatment with NaOH generates a bioactive surface with nanometer-scale roughness having a high specific surface area, but the sodium titanate formed by this treatment may have an undesirable effect on living cells in the narrow spaces of the porous material by the release Na^+ ions. In contrast, treatment with acid generates a bioactive surface with micrometer-scale roughness having a low specific surface area, but the TiO_2 formed by this treatment does not release ions that are liable to have adverse effects on living cells. Recently, it was shown that when Ti metal is subjected to HCl and heat treatment [21] subsequent to NaOH treatment, the bioactive TiO_2 layer that was formed had nanometer-scale roughness with a high specific surface area and releases no ions. In addition, porous Ti metal that

had been subjected to these treatments exhibited higher values of osteoconductivity and osteoinductivity than that subjected to simple NaOH and heat treatment [22–25].

In this study, we investigated the type of acid treatment that would be effective for inducing high apatite-forming ability of TiO_2 formed on Ti metal. Treatment with NaOH, acid, and heat were investigated. Factors governing their apatite-forming abilities were discussed in terms of their surface structure and properties.

Several articles that investigate the apatite-forming ability of TiO_2 that is formed on Ti metal by various treatment methods have been published [26–36]. However, the principal factors governing apatite formation on TiO_2 are not yet clearly understood.

2 Materials and methods

2.1 Preparation of the samples

Commercially pure Ti metal (Kobe Steel, Ltd, Japan) was cut into rectangular samples with dimensions of 10 × 10 × 1 mm^3, abraded with a #400 diamond plate, washed with acetone, 2-propanol, and ultra pure water for 30 min each in an ultrasonic cleaner, and then dried overnight in an oven at 40°C. Each sample was soaked in 5 ml of a 5 M NaOH solution at 60°C in an oil bath, shaken at 120 strokes/min for 24 h, and then gently washed with ultra pure water. Subsequently, the samples were soaked in 10 ml of an HCl, HNO_3, or H_2SO_4 solution with concentrations ranging from 0.5 to 100 mM at 40°C in an oil bath, shaken at 120 strokes/min for 24 h, and then gently washed with ultra pure water and dried overnight in an oven at 40°C. The samples were heated to 600°C at a rate of 5°C/min in an Fe–Cr electric furnace, maintained at this temperature for 1 h, and then cooled naturally to room temperature in the furnace.

2.2 Surface analysis of the treated Ti metal

The surface of the Ti metal treated as described above was analyzed using thin film X-ray diffraction (TF-XRD, RINT-2500, Rigaku Co., Japan). The X-ray source used was CuKα, and the angle of the incident beam was set to 1° against the sample surface. The same surface was coated with a Pt/Pd film and observed under a field emission scanning electron microscope (FE-SEM, Hitachi S-4300, Hitachi, Japan).

Ti metal plates with dimensions of 13 × 33 × 1 mm^3 were used to measure the zeta potential, and in the NaOH and acid treatments of the samples, the volumes of the NaOH and acid solutions used were increased to 20 and 30 ml, respectively. The treated Ti metal plates were electrically grounded to discharge any stray charges, and were immediately set in the zeta potential and particle size analyzer (ELS-Z1, Otsuka Electronics Co., Japan) using a glass cell for the plate sample. The zeta potential of the samples was measured under an applied voltage of 40 V in a 10 mM NaCl solution dispersing monitor particles of polystyrene latex particles (diameter = 500 nm) coated with hydroxyl propyl cellulose. Five samples were measured for each experimental condition, and the average value was used in our analysis.

2.3 Examination of the apatite-forming ability in a simulated body fluid (SBF)

The Ti metals treated as described above were soaked in 30 ml of an acellular SBF at 36.5°C with ion concentrations (Na^+ = 142.0, K^+ = 5.0, Mg^{2+} = 1.5, Ca^{2+} = 2.5, Cl^- = 147.8, HCO_3^- = 4.2, HPO_4^{2-} = 1.0, and SO_4^{2-} = 0.5 mM) nearly equal to those of human blood plasma. The SBF was prepared by dissolving reagent-grade NaCl, $NaHCO_3$, KCl, $K_2HPO_4{\cdot}3H_2O$, $MgCl_2{\cdot}6H_2O$, $CaCl_2$, and Na_2SO_4 (Nacalai Tesque Inc., Japan) in ultra pure water, and buffering at pH = 7.40 using tris (hydroxymethyl) aminomethane [$(CH_2OH)_3CNH_2$] and 1 M HCl (Nacalai Tesque Inc.) [37].

After soaking for periods of 1 min and 12 h, the samples were removed from the SBF, gently washed with ultra pure water for 5 min and dried at 40°C in an oven. The sample's surface was analyzed using X-ray photoelectron spectroscopy (XPS, ESCA-3300KM, Shimadzu Co., Japan) using MgKα radiation (λ = 9.8903 Å) as the X-ray source. The XPS take-off angle was set at 45°, which enabled the system to detect photoelectrons to a depth of 5–10 nm from the surface of the substrate. The binding energy of the measured spectra was calibrated by reference to the C_{1S} peak of the surfactant's CH_2 group on the substrate occurring at 284.6 eV.

After soaking in the SBF for 1 day, the surface was analyzed for apatite formation using TF-XRD and FE-SEM. To examine the stability of the apatite-forming ability in a humid environment, the NaOH, acid, and heat-treated samples were kept at a relative humidity of 95% at 80°C for 1 week, and the apatite formed on their surface in the SBF was examined using FE-SEM.

3 Results

3.1 Surface structure of the treated Ti metals

Figure 1 shows FE-SEM photographs of the surface of Ti metals subjected to various acid treatments after an NaOH treatment, compared with the surface of untreated Ti metal

and that treated with an NaOH solution. The treatments shown in Fig. 1 are designated according to the classifications shown in Table 1. A fine network structure of nanometer-scale was generated on the surface of the Ti metal by an initial NaOH treatment, and this remained essentially unchanged after a subsequent acid treatment, as long as the acid concentration was not high. The network structure was completely dissolved by treatment with a concentrated acid solution. The maximum concentration of the acid solution in which the fine network structure remained was 50 mM for the HCl and HNO_3 solutions, and 10 mM for the H_2SO_4 solution.

Figure 2 shows FE-SEM photographs of the surface of Ti metals subjected to a heat treatment after an NaOH and acid treatment. The surface structure formed on the Ti metals by the NaOH and acid treatments remained essentially unchanged after the heat treatment.

Figures 3 and 4 show the TF-XRD patterns of the surface of Ti metals subjected to NaOH and acid treatments, and those of Ti metals subjected to a subsequent heat treatment, respectively. From Fig. 3, it can be seen that a layer of sodium hydrogen titanate ($Na_xH_{2-x}Ti_3O_7$, $0 < x < 2$) had formed on the surface of Ti metal after the initial NaOH treatment [38], and that this was converted to

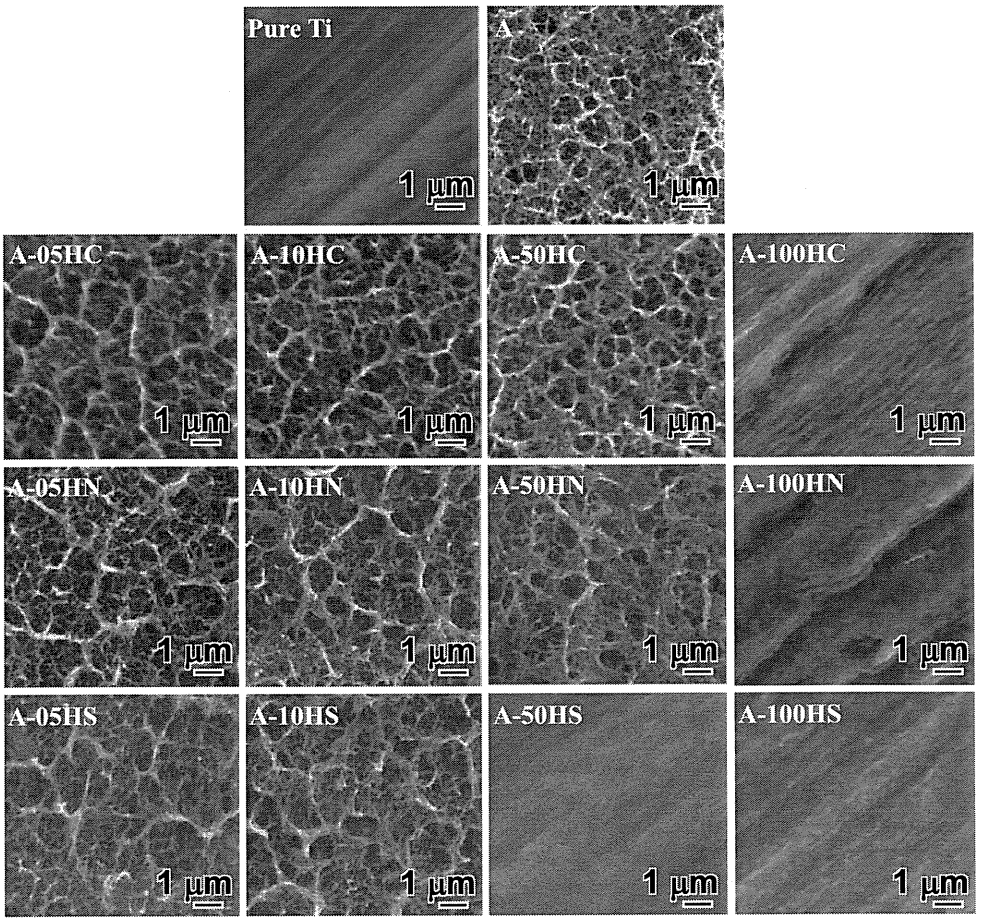

Fig. 1 FE-SEM photographs of surfaces of Ti metals subjected to various acid treatments after NaOH treatment, in comparison with those of Ti metal untreated and as-treated with NaOH. Explanation of notation is given in Table 1

Table 1 Notation of treatments

Notation	Treatments
A	Only NaOH treatment
A-05, 10, 50, or 100HC	A + 0.5, 10, 50 or 100 mM HCl treatments
A-05, 10, 50, or 100HC–H	A + 0.5, 10, 50 or 100 mM HCl + heat treatments
A-05, 10, 50, or 100HN	A + 0.5, 10, 50 or 100 mM HNO_3 treatments
A-05, 10, 50, or 100HN–H	A + 0.5, 10, 50 or 100 mM HNO_3 + heat treatments
A-05, 10, 50, or 100HS	A + 0.5, 10, 50 or 100 mM H_2SO_4 treatments
A-05, 10, 50, or 100HS–H	A + 0.5, 10, 50 or 100 mM H_2SO_4 + heat treatments

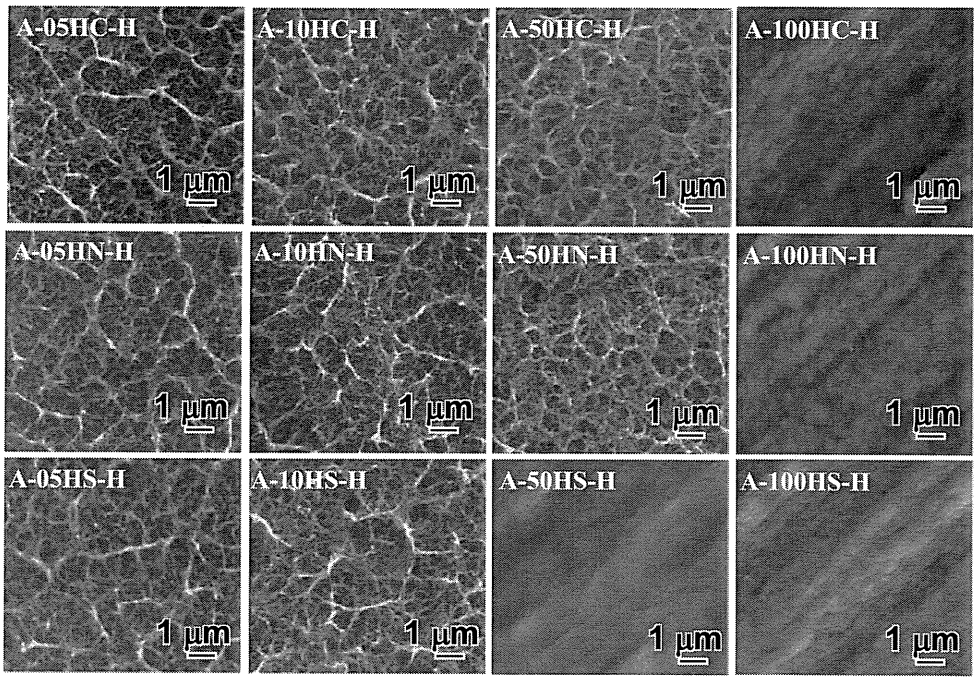

Fig. 2 FE-SEM photographs of surfaces of Ti metal subjected to the heat treatment after the acid and NaOH treatments, in comparison with those of Ti metal subjected to heat treatment without and after the NaOH treatment

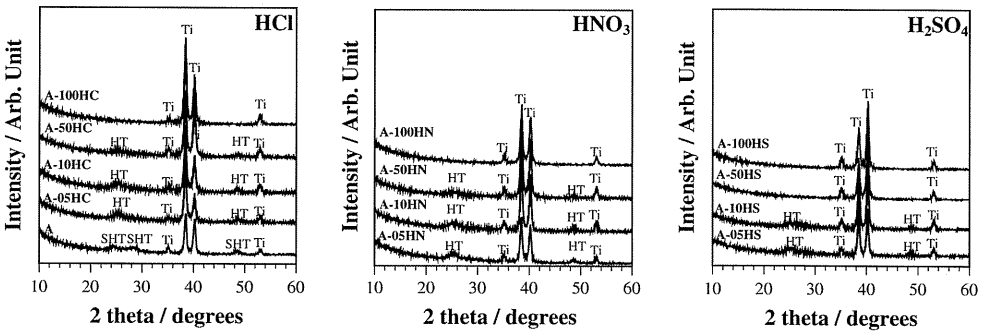

Fig. 3 TF-XRD of surfaces of Ti metal subjected to different chemical treatments. *Ti* α Ti, *HT* Hydrogen titanate, *SHT* Sodium hydrogen titanate

hydrogen titanate ($H_2Ti_3O_7$) [39] after a subsequent acid treatment, if the concentration of the acid solution was not high. After treatment with concentrated acid solutions, the sodium hydrogen titanate layer was completely dissolved. All the NaOH- and acid-treated Ti metals precipitated TiO_2 of anatase and/or rutile after the heat treatment (Fig. 4). The ratio of rutile to anatase increased with increasing concentration of the acid solution. Only the rutile phase was observed for the HCl and HNO_3 solutions with a concentration of 100 mM, and H_2SO_4 solutions with a concentration of 50 and 100 mM.

3.2 Apatite-forming ability of treated Ti metals in an SBF

Figures 5 and 6 show FE-SEM photographs of the surface of Ti metals soaked in an SBF for 1 day after different chemical treatments and a subsequent heat treatment, respectively. Spherical particles were observed on the surface, and these were identified as crystalline apatite from the TF-XRD data. Ti metals subjected to the chemical treatment alone did not form (or only formed a little) apatite on their surface in an SBF within a period of 1 day (Fig. 5). In contrast, all the Ti metals subjected to a heat treatment after a chemical treatment formed appreciable amounts of apatite on their surfaces in an SBF within 1 day (Fig. 6). The apatite-forming ability of the samples was high when the concentration of the acid solution used was greater than 10 mM.

Figure 7 shows FE-SEM photographs of the surface of Ti metals soaked in an SBF for 1 day after being kept at a relative humidity of 95% at 80°C for 1 week following NaOH, acid, and heat treatments. From Fig. 7, it can be seen that a high apatite-forming ability of such treated Ti metals was maintained, even in a humid environment.

3.3 Zeta potential of treated Ti metals

The zeta potentials of Ti metals treated with an acid solution after an NaOH treatment were not able to be

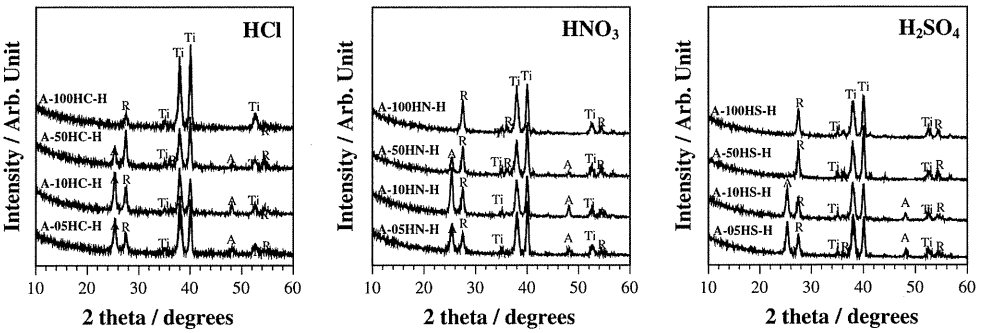

Fig. 4 TF-XRD of surfaces of Ti metal subjected to the heat treatment after different chemical treatments. *Ti* α Ti, *A* Anatase, *R* Rutile, *ST* Sodium titanate

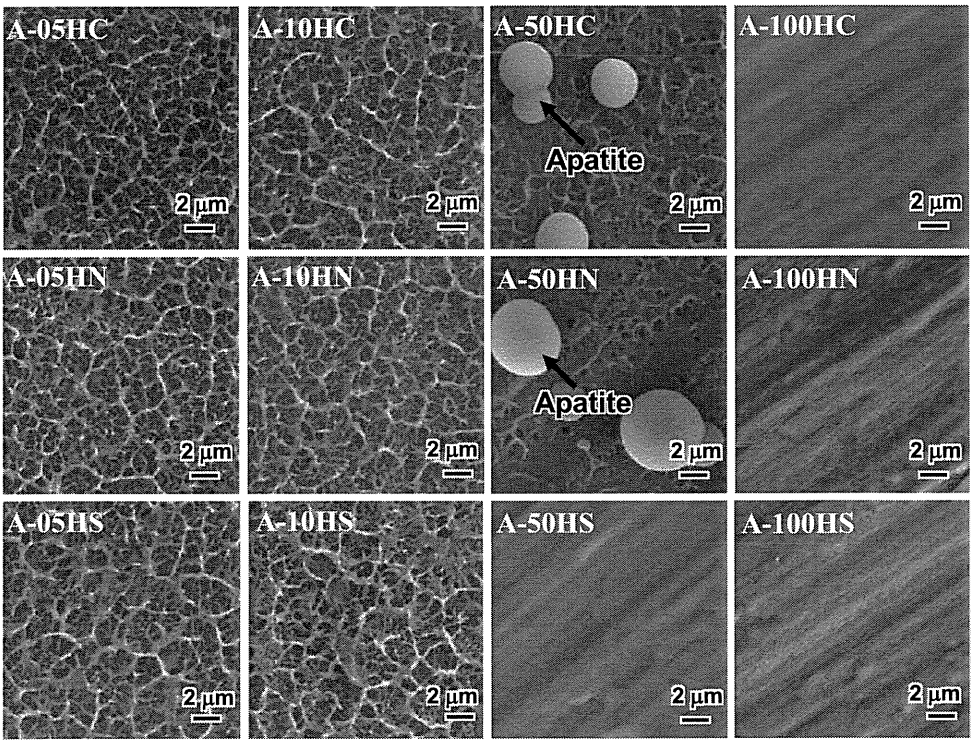

Fig. 5 FE-SEM photographs of surfaces of Ti metals soaked in SBF for 1 day after different chemical treatments

measured, as no insulating TiO_2 layer formed. This indicates that the zeta potential of these samples was almost zero. Figure 8 shows the zeta potentials of Ti metals subjected to a heat treatment after an NaOH and acid treatment. All the heat-treated samples showed a positive zeta potential, although the zeta potentials of Ti metals treated with 0.5 mM acid solutions were as low as 4 mV.

3.4 XPS spectra of treated Ti metals

Figure 9 shows the Ca_{2P} and P_{2P} XPS spectra of the surfaces of Ti metals soaked in an SBF for 1 min and 12 h after NaOH, acid, and heat treatments. From Fig. 9, it can be seen that all the treated Ti metals selectively adsorbed phosphate ions on their surface in an SBF within a period of 1 min, and later on, also adsorbed calcium ions to form calcium phosphate.

Figure 10 shows the Cl_{2P} and N_{1S} XPS spectra of the surfaces of Ti metal subjected to a heat treatment following an NaOH and 50 mM HCl or HNO_3 treatment. Also shown are the S_{2P} spectra of the surfaces of Ti metal treated with a 10 mM H_2SO_4 solution after an NaOH treatment after being subjected to a subsequent heat treatment and then kept at a relative humidity of 95% at 80°C for 1 week. From Fig. 10, it can be seen that chloride, nitrate, and sulfate ions were observed on the surface of Ti metals heat-treated after an HCl, HNO_3, and H_2SO_4 treatment following an NaOH treatment. Sulfate ions were detected on the surface of the samples before the heat treatment, and even after being kept in a humid environment for 1 week.

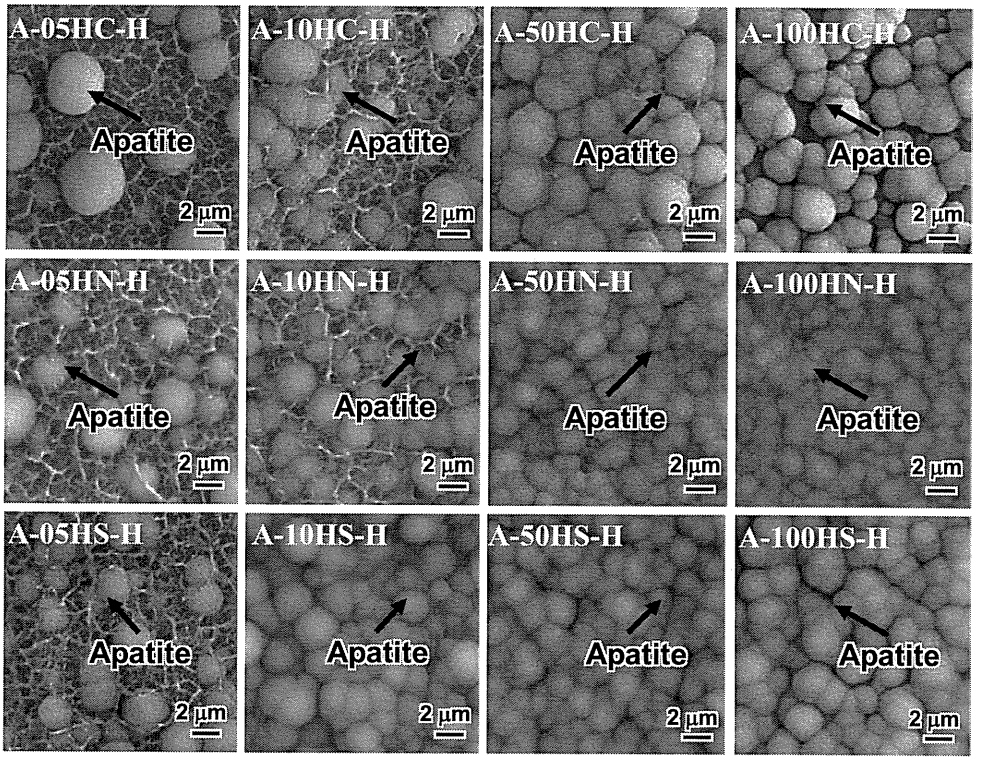

Fig. 6 FE-SEM photographs of surfaces of Ti metals soaked in SBF for 1 day after heat treatment following different chemical treatments

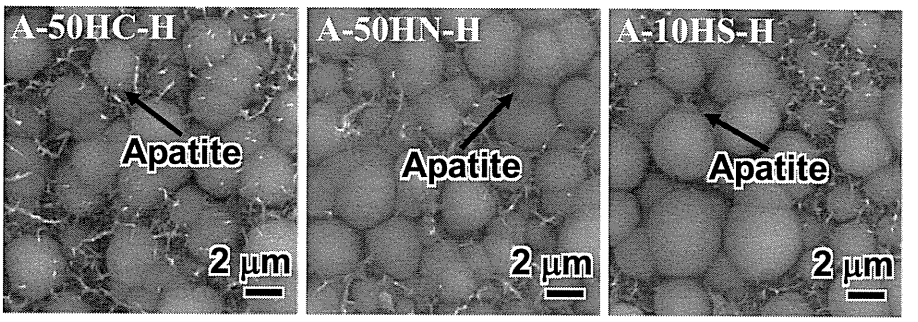

Fig. 7 FE-SEM photograph of surface of Ti metals soaked in SBF for 1 day, after kept in humid environment for 1 week following the NaOH, acid and heat treatments

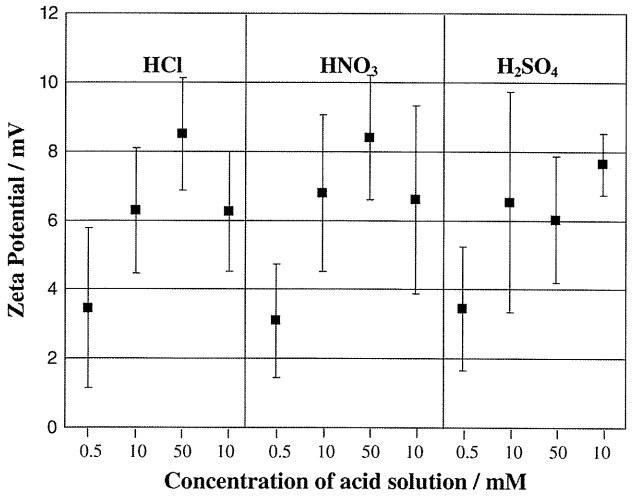

Fig. 8 Zeta potentials of surfaces of Ti metal plates after different chemical and heat treatments

4 Discussion

It is apparent from Figs. 1 and 2 that a nanometer-scale roughness is generated on the surface of Ti metals by an NaOH treatment and remained after the subsequent acid and heat treatments as long as the acid concentration is not high.

According to Figs. 3 and 4, sodium hydrogen titanate formed on Ti metals by an NaOH treatment is transformed into hydrogen titanate or completely dissolved by the subsequent acid treatment and then transformed into TiO_2 of anatase and/or rutile by the heat treatment.

It is apparent from Figs. 5 and 6 that the apatite-forming ability in an SBF of Ti metals subjected to an acid treatment after an NaOH treatment was very low before a heat treatment, but increased markedly after a heat treatment, irrespective of the type of acid solution used.

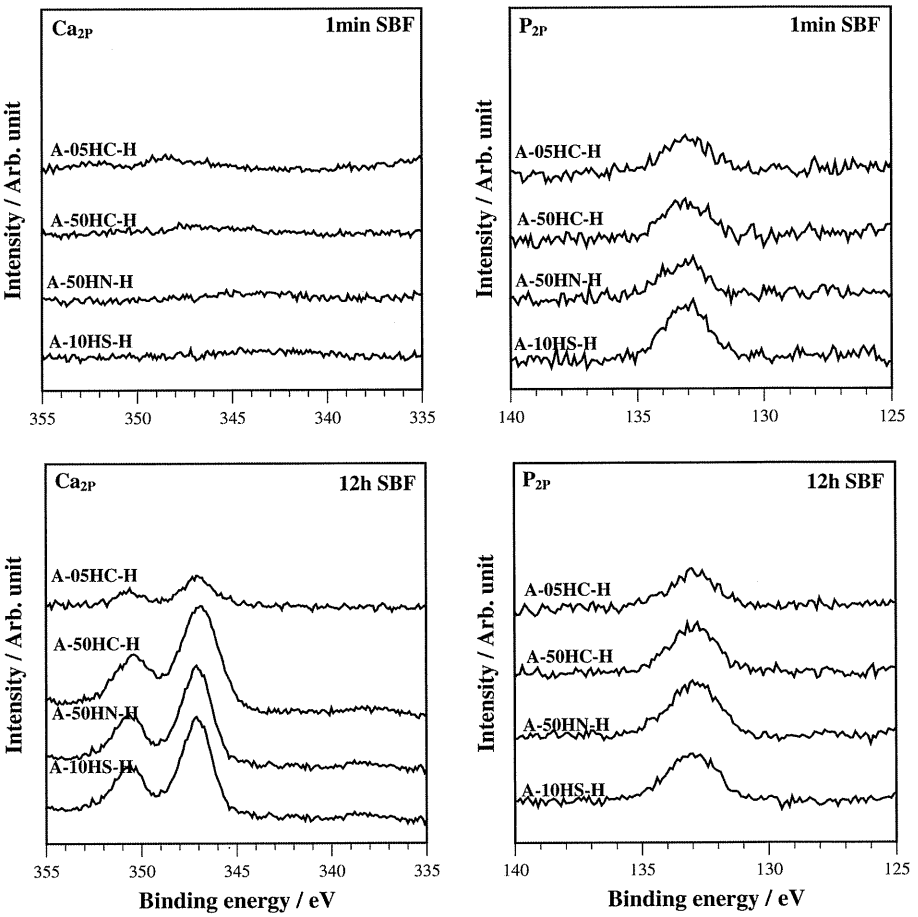

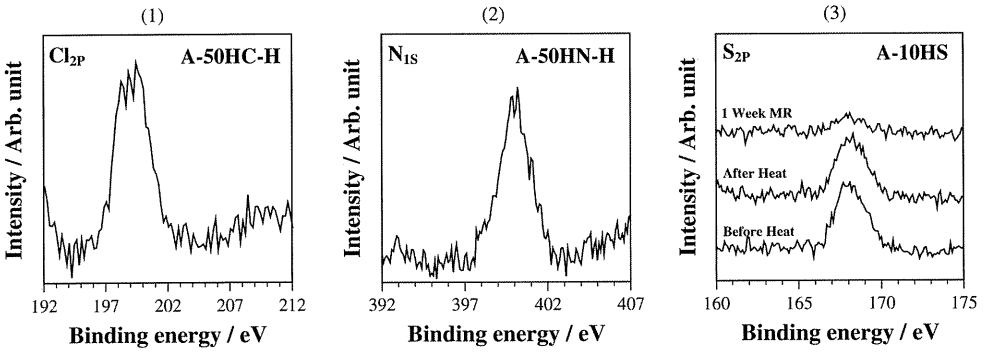

Fig. 9 XPS spectra of surfaces of Ti metals soaked in SBF for 1 min and 12 h after different chemical and heat treatments

Fig. 10 XPS spectra of surfaces of Ti metals subjected to various chemical and heat treatments. *1* after heat treatment following NaOH and 50 mM HCl treatment; *2* after heat treatment following NaOH and 50 mM HNO_3 treatment; *3* before and after heat treatment following the NaOH and 10 mM H_2SO_4 treatment, and after subsequent storage in 95% relative humidity at 80°C for 1 week

As described above, the surface roughness of Ti metal subjected to an acid treatment after an NaOH treatment did not change after a heat treatment. Therefore, the increase in the apatite-forming ability after the heat treatment cannot be attributed to the change in surface roughness.

As described above, the surface phase of the Ti metals subjected to an acid treatment after an NaOH treatment was either hydrogen titanate or titanium before the heat treatment, while it was TiO_2 of anatase and/or rutile after the heat treatment. This indicates that TiO_2 is responsible for the high apatite-forming ability of the heat-treated Ti metal. However, apatite-forming ability of the heat-treated Ti metal does not depend upon the type of TiO_2 formed. For example, Ti metal treated with a 10 mM H_2SO_4 solution showed an almost equal apatite-forming ability to that of sample treated with a 100 mM H_2SO_4 solution (see

Fig. 6), although the former sample had a larger amount of anatase precipitated than rutile, whereas the latter sample had precipitated only rutile (see Fig. 4). Therefore, the apatite-forming ability of the heat-treated Ti metal samples cannot be attributed to the specific crystalline phase of TiO_2 precipitated.

The zeta potential of Ti metals subjected to an acid solution after an NaOH treatment was almost zero before a heat treatment, as described above. According to Fig. 8, the zeta potential of Ti metals subjected to an acid treatment after an NaOH treatment showed positive values after the heat treatment, and high values were observed when the concentration of the acid solution was greater than 10 mM, irrespective of the type of acid solution used. Figures 5 and 6 show that the apatite-forming ability of Ti metals subjected to an acid treatment after an NaOH treatment was increased by the heat treatment and became high when the concentration of the acid solution was greater than 10 mM, irrespective of the type of acid solution used.

When Ti metals have a positively charged surface, then negatively charged phosphate ions can be selectively adsorbed on their surface first. As these phosphate ions accumulate, the surface becomes negatively charged. As a result, positively charged calcium ions can be adsorbed on the surface to produce apatite. This sequential adsorption of phosphate and calcium ions was confirmed in the XPS spectra of Ti metals heat-treated after various acid treatments shown in Fig. 9. From these observations, it can be concluded that the high apatite-forming ability of the Ti metals heat-treated after an acid treatment following an NaOH treatment can be attributed to their positive surface charge.

The reason why the Ti metals heat-treated after an acid treatment following an NaOH treatment had a positive surface charge can be interpreted in terms of the acid groups adsorbed on their surface after the acid treatment. It was confirmed by the XPS spectra shown in Fig. 10 that sulfate ions were adsorbed on Ti metal soaked in an H_2SO_4 solution after an NaOH treatment, and that these remained on the Ti metal surface, even after subsequent heat treatment. Chloride ions and nitrate ions were also confirmed to be adsorbed on the Ti metal heat-treated after treatment in an HCl and HNO_3 solution, as shown in Fig. 10. These acid groups can dissociate from the surface of the Ti metals in an SBF to give an acidic surface environment. TiO_2 has been reported to be positively charged in acidic aqueous solutions, and its positive charge increases with decreasing pH of the solution [40, 41]. The acid solutions used in this study had pH values that decreased with increasing acid concentration, as shown in Table 2. All the acid solutions used in this study had pH values lower than 2 when their concentration was greater than 10 mM.

Table 2 pH values of acid solutions used in the present study

Solution	pH			
	0.5 mM	10 mM	50 mM	100 mM
HCl	3.46	2.13	1.47	1.16
HNO_3	3.50	2.14	1.46	1.15
H_2SO_4	3.10	1.98	1.25	1.05

The acid groups adsorbed on the Ti metals heat-treated after an acid treatment remained, even after the Ti metals were stored in a humid environment at high temperature, as shown in Fig. 10. Therefore, their high apatite-forming ability was maintained, even after storage in a humid environment at high temperature (see Fig. 7).

We have shown in a separate article that Ti metal heat-treated after H_2SO_4/HCl mixed acid treatment without being subjected to NaOH treatment formed TiO_2 layer [20] that formed apatite on its surface in a body environment and tightly bonded to living bone. The formation of apatite on the surface was also attributed to positive surface charge [20]. Our present results show that apatite formation induced by the positive surface charge of the Ti metal heat-treated after acid treatment is not specific to the use of a mixed acid solution, but is independent of the type of acid solution used, and is also independent of the surface condition before the acid treatment.

It has been shown previously that a porous Ti metal heat-treated after an HCl treatment following an NaOH treatment exhibits high osteoconductivity [22, 42] as well as osteoinductivity [23, 24]. This type of bioactive porous Ti metal is now being subjected to clinical trials for application in spinal fusion devices after animal experiment [25]. Our results provide a contribution to the development of porous Ti metals with higher osteoconductivity and osteoinductivity.

5 Conclusions

Nanometer-scale roughness was generated on the surface of Ti metal by NaOH treatment and remained even after formation of titanium oxide by the subsequent acid and heat treatments, as long as the acid concentration was not high. Ti metal treated with HCl, HNO_3 and H_2SO_4 solutions after an NaOH treatment showed high apatite-forming ability in an SBF after a subsequent heat treatment, especially when the acid concentration was greater than 10 mM. This was not attributed to either the surface roughness induced by the chemical treatment or to the specific crystalline phase precipitated on the Ti metal, but to the positive surface charge of the TiO_2 precipitated on the Ti metal by the acid and heat treatments. The positively

charged Ti metals first adsorbed the negatively charged phosphate ions in an SBF, and then the positively charged calcium ions to form apatite on their surface.

Such treated Ti metals are expected to form apatite on their surface in a short period, even in a living body, and can bond to living bone through this apatite layer. These findings will contribute to the development of porous Ti metal with higher osteoconductivity and osteoinductivity.

Acknowledgments The present authors acknowledge Prof. Y. Taga of Chubu University, Japan for his assistance in the XPS measurements. Useful suggestions by Dr. T. Kizuki and Prof. H. Takadama of Chubu University are also acknowledged.

References

1. Hanawa T, Kamimura Y, Yamamoto S, Kohgo T, Amemiya A, Ukai M, Murakami H, Asaoka K. Early bone formation around calcium-ion-implanted titanium inserted into rat tibia. J Biomed Mater Res. 1997;36:131–6.
2. Armitage DA, Mihoc R, Tate TJ, McPhail DS, Chater R, Hobkirk JA, Shinawi L, Jones FH. The oxidation of calcium implanted titanium in water: a depth profiling study. Appl Surf Sci. 2007; 253:4085–93.
3. Nayab SH, Jones FH, Olsen I. Effect of calcium ion implantation on bone cell function in vitro. J Biomed Mater Res. 2007;83A: 296–302.
4. Sul YT. The significance of the surface properties of oxidized titanium to the bone response: special emphasis on potential biochemical bonding of oxidized titanium implant. Biomaterials. 2003;24:3893–4007.
5. Song WH, Ryu HS, Hong SH. Apatite induction on Ca-containing titania formed by micro-arc oxidation. J Am Ceram Soc. 2005;88:2642–4.
6. Frojd V, Franke-Stenport V, Meirelles L, Wennerberg A. Increased bone contact to a calcium-incorporated oxidized commercially pure titanium implant: an in vivo study in rabbits. Int J Oral Maxillofac Surg. 2008;37:561–6.
7. Wu J, Liu ZM, Zhao XH, Gao Y, Hu J, Gao B. Improved biological performance of microarc-oxidized low-modulus Ti–24Nb–4Zr–7.9Sn alloy. J Biomed Mater Res. 2010;92B:298–306.
8. Whiteside P, Matykina E, Gough JE, Skeldon P, Thompson GE. In vitro evaluation of cell proliferation and collagen synthesis on titanium following plasma electrolytic oxidation. J Biomed Mater Res. 2010;94A:38–46.
9. Nakagawa M, Zhang L, Udoh K, Matsuya S, Ishikawa K. Effects of hydrothermal treatment with $CaCl_2$ solution on surface property and cell response of titanium implants. J Mater Sci. 2005;16:985–91.
10. Park JW, Park KB, Suh JY. Effects of calcium ion incorporation on bone healing of Ti6Al4V alloy implants in rabbit tibiae. Biomaterials. 2007;28:3306–13.
11. Ueda M, Ikeda M, Ogawa M. Chemical–hydrothermal combined surface modification of titanium for improvement of osteointegration. J Mater Sci Eng C. 2009;29:994–1000.
12. Chen XB, Li YC, Plessis JD, Hodgson PD, Wen C. Influence of calcium ion deposition on apatite-inducing ability of porous titanium for biomedical applications. Acta Biomater. 2009;5:1808–20.
13. Park JW, Kim YJ, Jang JH, Kwon TG, Bae YC, Suh JY. Effects of phosphoric acid treatment of titanium surfaces on surface properties, osteoblast response and removal of torque forces. Acta Biomater. 2010;6:1661–70.
14. Kokubo T, Miyaji F, Kim HM, Nakamura T. Spontaneous formation of bone-like apatite layer on chemically treated titanium metals. J Am Ceram Soc. 1996;79:1127–9.
15. Kim HM, Miyaji F, Kokubo T, Nakamura T. Preparation of bioactive Ti and its alloy via simple chemical surface treatment. J Biomed Mater Res. 1996;32:409–17.
16. Yan WQ, Nakamura T, Kobayashi M, Kim HM, Miyaji F, Kokubo T. Bonding of chemically treated titanium implants to bone. J Biomed Mater Res. 1997;37:267–75.
17. Yan WQ, Nakamura T, Kawanabe K, Nishiguchi S, Oka M, Kokubo T. Apatite layer-coated titanium for use as bone bonding implants. Biomaterials. 1997;18:1185–90.
18. Nishiguchi S, Fujibayashi S, Kim HM, Kokubo T, Nakamura T. Biology of alkali- and heat-treated titanium implants. J Biomed Mater Res. 2003;67A:26–35.
19. Kawanabe K, Ise K, Goto K, Akiyama H, Nakamura T, Kaneuji A, Sugimori T, Matsumoto T. A new cementless total hip arthoplasty with bioactive titanium porous-coating by alkaline and heat treatment: average 4.8-year results. J Biomed Mater Res. 2009;90B:476–81.
20. Kokubo T, Pattanayak DK, Yamaguchi S, Takadama H, Matsushita T, Kawai T, Takemoto M, Fujibayashi S, Nakamura T. Positively charged bioactive titanium metal prepared by simple chemical and heat treatments. J R Soc Interface. 2010;7:S503–13.
21. Pattanayak DK, Kawai T, Matsushita T, Takadama H, Nakamura T, Kokubo T. Effect of HCl concentrations on apatite-forming ability of NaOH–HCl– and heat-treated titanium metal. J Mater Sci: Mater Med. 2009;20:2401–11.
22. Fujibayashi S, Neo M, Kim HM, Kokubo T, Nakamura T. Osteoinduction of porous bioactive titanium metal. Biomaterials. 2004;25:443–50.
23. Takemoto M, Fujibayashi S, Neo M, Suzuki J, Kokubo T, Nakamura T. Mechanical properties and osteoconductivity of porous bioactive titanium. Biomaterials. 2005;26:6014–23.
24. Takemoto M, Fujibayashi S, Neo M, Suzuki J, Matsushita T, Kokubo T, Nakamura T. Osteoinductive porous titanium implants: effect of sodium removal by dilute HCl treatment. Biomaterials. 2006;27:2682–91.
25. Takemoto M, Fujibayashi S, Neo M, So K, Akiyama N, Matsushita T, Kokubo T, Nakamura T. A porous bioactive titanium implant for spinal inter body fusion: an experimental study using a canine model. J Neurosurg Spine. 2007;7:435–43.
26. Uchida M, Kim HM, Kokubo T, Fujibayashi S, Nakamura T. Effect of water treatment on the apatite-forming ability of NaOH-treated titanium metal. J Biomed Mater Res. 2002;63:522–30.
27. Wang XX, Hayakawa S, Tsuru K, Osaka A. Bioactive titania gel layers formed by chemical treatment of Ti substrate with a H_2O_2/HCl solution. Biomaterials. 2002;23:1353–7.
28. Wang XX, Yan W, Hayakawa S, Tsuru K, Osaka A. Apatite deposition on thermally and anodically oxidized titanium surfaces in a simulated body fluid. Biomaterials. 2003;24:4631–7.
29. Yang B, Uchida M, Kim HM, Zhang X, Kokubo T. Preparation of bioactive titanium metal via anodic oxidation treatment. Biomaterials. 2004;25:1003–10.
30. Rohanizadeh R, Al-Sadeq M, LeGeros RZ. Preparation of different forms of titanium oxide on titanium surface: effects on apatite deposition. J Biomed Mater Res. 2004;71A:343–52.
31. Wu JM, Hayakawa S, Tsuru K, Osaka A. Low-temperature preparation of anatase and rutile layers on titanium substrates and their ability to induce in vitro apatite deposition. J Am Ceram Soc. 2004;87:1635–42.
32. Lu X, Zhao Z, Leng Y. Biomimetic calcium phosphate coatings on nitric acid treated titanium surfaces. J Mater Sci Eng C. 2007;27:700–8.

33. Lee MH, Park IS, Min KS, Ahn SG, Park JM, Song KY, Park CW. Evaluation of in vitro and in vivo tests for surface modified titanium by H_2SO_4 and H_2O_2 treatment. Met Mater Int. 2007;13:109–15.
34. Lu X, Wang Y, Yang X, Zhang Q, Zhao Z, Weng LT, Leng Y. Spectroscopic analysis of titanium surface functional groups under various surface modification and their behaviors in invitro and invivo. J Biomed Mater Res. 2008;84A:523–34.
35. Lindberg F, Heinrichs J, Ericson F, Thomsen P, Engqvist H. Hydroxylapatite growth on single-crystal rutile substrates. Biomaterials. 2008;29:3317–23.
36. Sugino A, Ohtsuki C, Tsuru K, Hayakawa S, Nakano T, Okazaki Y, Osaka A. Effect of spatial design and thermal oxidation on apatite formation on Ti–15Zr–4Ta–4Nb alloy. Acta Biomater. 2009;5:298–304.
37. Kokubo T, Takadama H. How useful is SBF in predicting in vivo bone bioactivity? Biomaterials. 2006;27:2907–15.
38. Sun X, Li Y. Synthesis and characterization of ion-exchangeable titanate nanotubes. Chem Eur J. 2003;9:2229–38.
39. Tsai CC, Teng H. Structural features of nanotubes synthesized from NaOH treatment on TiO_2 with different post-treatments. Chem Mater. 2006;18:367–73.
40. Textor M, Sittig C, Frauchiger V, Tosatti S, Brunette DM. Properties and biological significance of natural oxide films on titanium and its alloys. In: Brunette DM, Tengvall P, Textor M, Thomsen P, editors. Titanium in medicine. Germany: Springer; 2001. p. 171–230.
41. Kokubo T, Takagi H, Tashiro M. Alkaline durability of BaO–TiO_2–SiO_2 glasses. J Non Cryst Solids. 1982;52:427–33.
42. Fujibayashi S, Nakamura T, Nishiguchi S, Tamura J, Uchida M, Kim HM, Kokubo T. Bioactive titanium: effect of sodium removal on the bone-bonding ability of bioactive titanium prepared by alkali and heat treatment. J Biomed Mater Res. 2001; 56:562–70.

J Mater Sci: Mater Med (2011) 22:273–278
DOI 10.1007/s10856-010-4218-y

Effect of heat treatments on apatite-forming ability of NaOH- and HCl-treated titanium metal

Deepak K. Pattanayak · Seiji Yamaguchi · Tomiharu Matsushita · Tadashi Kokubo

Received: 6 October 2010 / Accepted: 11 December 2010 / Published online: 29 December 2010

Abstract Titanium (Ti) metal was soaked in HCl solution after NaOH treatment and then subjected to heat treatments at different temperatures. Their apatite-forming abilities in a simulated body fluid (SBF) were discussed in terms of their surface structures and properties. The nanometer scale roughness formed on Ti metal after NaOH treatment remained after the HCl treatment and a subsequent heat treatment below 700°C. Hydrogen titanate was formed on Ti metal from an HCl treatment after NaOH treatment, and this was converted into titanium oxide of anatase and rutile phases by a subsequent heat treatment above 500°C. The scratch resistance of the surface layer increased with the formation of the titanium oxide after a heat treatment up to 700°C, and then decreased with increasing temperature. The Ti metal with a titanium oxide layer formed on its surface showed a high apatite-forming ability in SBF when the heat treatment temperature was in the range 500–700°C. The high apatite-forming ability was attributed to the positive surface charge in an SBF. These positive surface charges were ascribed to the presence of chloride ions, which were adsorbed on the surfaces and dissociated in the SBF to give an acid environment.

1 Introduction

Titanium (Ti) metal and its alloys are widely used as various implants in orthopedic and dental fields because of their high mechanical strength and good biocompatibility [1]. However, they do not bond to living bone [2]. Early on, it was shown that Ti metal forms a bone-like apatite layer on its surface in the living body, and bonds to living bone through this apatite layer, if it is subjected to NaOH and heat treatment to form sodium titanate on its surface [3–6]. These treatments have been applied to the porous layer of an artificial hip joint and the resulting implant has been used clinically in Japan since 2007 [7].

Later it was also found that Ti metal forms the bone-like apatite on its surface in a simulated body fluid (SBF), even if it is soaked in water or HCl solution after the NaOH treatment and then heat-treated at 600°C to form titanium oxide on its surface [8]. Its apatite-forming ability increased with increasing concentration of the HCl solution, and assumed to be attributed to positive surface charge of the Ti metal increased with increasing concentration of the HCl solution [8].

In this study, Ti metal was soaked in 50 mM HCl solution after the NaOH treatment and then subjected to heat treatment at different temperatures. Their apatite-forming abilities in SBF were discussed in terms of their surface structures and properties. Much attention has been paid on bioactive Ti metal prepared by HCl and heat treatments after the NaOH treatment, because a porous Ti metal subjected to these treatments was found to exhibit osteoconductivity [9] as well as osteoinductivity [10]. It is already being subjected to clinical trial for application to spinal fusion devices [11].

2 Materials and methods

2.1 Preparation of specimens

Commercially pure Ti metal (Kobe Steel, Ltd., Japan) was cut into rectangular samples (dimensions = 10 × 10 × 1 mm^3),

D. K. Pattanayak (✉) · S. Yamaguchi · T. Matsushita · T. Kokubo
Department of Biomedical Sciences, College of Life and Health Sciences, Chubu University, 1200 Matsumoto-cho, Kasugai 487-8501, Japan
e-mail: deepak@isc.chubu.ac.jp; deepak_pattanayak@rediffmail.com

abraded with a #400 diamond plate, washed with acetone, 2-propanol, and ultrapure water for 30 min each in an ultrasonic cleaner, and then dried overnight in an oven at 40°C. The samples were then soaked in 5 ml of a 5 M NaOH solution at 60°C in an oil bath while being shaken at 120 strokes/min for a period of 24 h, and then gently washed with ultrapure water. Subsequently, the samples were soaked in 10 ml of a 50 mM HCl solution at 40°C in an oil bath while being shaken at 120 strokes/min for a period of 24 h. The samples were then gently washed with ultrapure water and dried overnight in an oven at 40°C. The samples were heated to several temperatures in the range 400–800°C at a rate of 5°C/min in Fe–Cr electric furnace in air, maintained at the desired temperature for a period of 1 h, and then allowed to cool at the natural rate of the furnace to room temperature. For the present study, ten samples were prepared in each heat treatment condition.

2.2 Examination of the apatite-forming ability in an SBF

The samples subjected to NaOH, HCl, and heat treatments were soaked at 36.5°C in 30 ml of an acellular SBF with ion concentrations nearly equal to those of human blood plasma (Na^+ 142.0, K^+ 5.0, Mg^{2+} 1.5, Ca^{2+} 2.5, Cl^- 147.8, HCO_3^- 4.2, HPO_4^{2-} 1.0, and SO_4^{2-} 0.5 mM). The SBF was prepared by dissolving reagent grade NaCl, $NaHCO_3$, KCl, $K_2HPO_4{\cdot}3H_2O$, $MgCl_2{\cdot}6H_2O$, $CaCl_2$, and Na_2SO_4 (Nacalai Tesque, Inc., Japan) in ultrapure water, and the solution was buffered at pH = 7.40 using tris (hydroxymethyl) aminomethane [$(CH_2OH)_3CNH_2$] and 1 M HCl (Nacalai Tesque, Inc.) [12]. The samples were removed from the SBF after 1 day, gently washed with ultrapure water, and dried in an oven at 40°C. The formation of apatite on the surface of the samples was examined using scanning electron microscopy (SEM) and thin film X-ray diffraction (TF-XRD) using the methods described in the next section.

2.3 Surface analysis of treated Ti metals

The surface of the Ti metals subjected to NaOH, HCl, and heat treatments, and those subsequently soaked in an SBF for several periods were analyzed using TF-XRD (TF-XRD; RINT-2500, Rigaku Co., Japan) and X-ray photoelectron spectroscopy (XPS; ESCA-3300KM, Shimadzu Co., Japan). In the TF-XRD experiments, CuKα radiation was used as the X-ray source, and the angle of the incident beam was 1° against the sample surface. In the XPS experiments, MgKα radiation was used as the X-ray source (λ = 9.8903 Å). The XPS takeoff angle was set at 45°, which enabled the system to detect photoelectrons to a depth of 5–10 nm from the surface of the substrate. The binding energy of the measured spectra was calibrated by reference to the C_{1s} peak of the surfactant's CH_2 group on the substrate occurring at 284.6 eV.

The sample surfaces were coated with a Pt/Pd film and observed under a field emission scanning electron microscope (FE-SEM; Hitachi S-4300, Hitachi Co., Japan) using an acceleration voltage of 15 kV.

The scratch resistance of the surfaces of the treated Ti metals was measured using a scratch tester (CSR-2000; Rhesca Co., Ltd., Japan). In this measurement, a stylus with diamond tip was moved on the sample surface at a speed of 10 mm/s under an applied load of 100 mN/min. The critical scratch load was estimated from an abrupt change in the signal of the sensor output, which indicated a complete peeling of the surface layer.

The zeta potential of the treated Ti metals was measured using plate samples (dimensions = 13 × 33 × 1 mm^3). In the preparation of these plate samples, 20 ml of the NaOH solution and 30 ml of the HCl solution were used. The Ti metal samples were first grounded to allow for leakage of any stray charge, and were then immediately set in a zeta potential and particle size analyzer (ELS-Z1, Otsuka Electronics Co., Japan) using a glass cell for the plate sample. The zeta potential was measured under an applied voltage of 40 V in a 10 mM NaCl solution with dispersed monitor particles composed of polystyrene latex particles (diameter = 500 nm) coated with hydroxyl propyl cellulose. Five samples were measured for each experimental condition, and the average values were used in the analysis.

3 Results

3.1 Surface structure of the treated Ti metal

Figure 1 shows FE-SEM photographs of the surface of Ti metal subjected to heat treatments at various temperatures after NaOH and HCl treatments. A fine network structure on the nanometer scale formed on the surface of the Ti metal after the initial NaOH treatment, and this remained essentially unchanged after the subsequent HCl and heat treatments up to 700°C, but began to fade for a heat treatment of 800°C.

Figure 2 shows the TF-XRD patterns of surface of Ti metal subjected to heat treatment at various temperatures after NaOH and HCl treatments. From Fig. 2, it can be seen that hydrogen titanate ($H_2Ti_3O_7$) had formed on the Ti metal surface after the NaOH and HCl treatments [8, 13, 14], and that this phase had converted to anatase and rutile after subsequent heat treatments above 500°C. The ratio of rutile to anatase increased with increasing heat treatment temperature, and only rutile was detected for a heat treatment temperature of 800°C.

Figure 3 shows the scratch resistance of the surface of Ti metal subjected to heat treatments at various

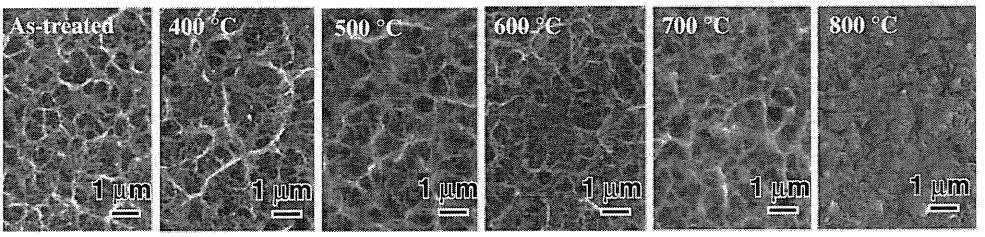

Fig. 1 FE-SEM photographs of surface of Ti metals subjected to heat treatments after NaOH and HCl treatments at various temperatures

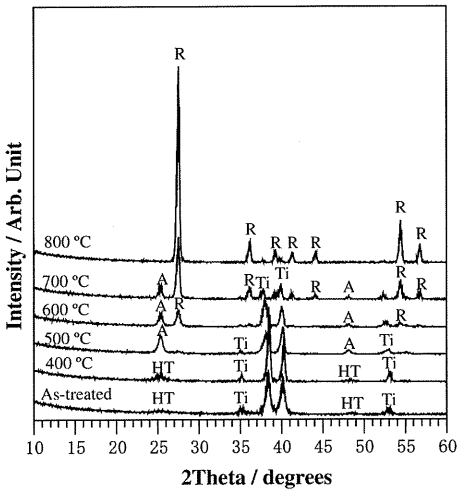

Fig. 2 TF-XRD patterns of surfaces of Ti metals subjected to heat treatments at various temperatures after NaOH and HCl treatments. *Ti* α Titanium, *HT* Hydrogen titanate, *A* anatase, *R* Rutile

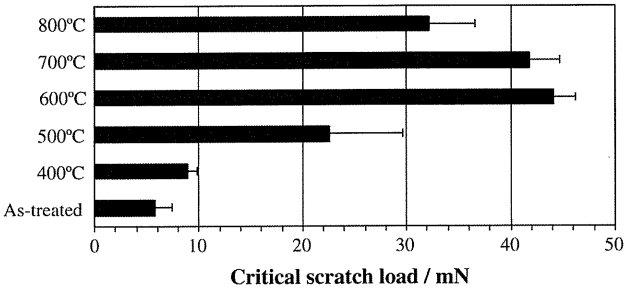

Fig. 3 Scratch resistances of surfaces of Ti metals subjected to heat treatments at various temperatures after NaOH and HCl treatments

temperatures after NaOH and HCl treatments. From Fig. 3, it can be seen that the scratch resistance of the surface of the Ti metal was as low as 5 mN after the NaOH and HCl treatments, and this increased to 45 mN with increasing heat treatment temperature up to 600°C, and that the scratch resistance decreased for heat treatment temperatures above 700°C.

3.2 Apatite-forming ability of treated Ti metal in an SBF

Figure 4 shows FE-SEM photographs of the surface of Ti metal soaked in an SBF for 1 day after heat treatment at various temperatures following NaOH and HCl treatments. A small number of spherical particles was observed on the surface of the Ti metal treated with NaOH and HCl solutions, and the number of these particles increased with increasing heat treatment temperature up to 700°C, and then decreased for a heat treatment temperature of 800°C.

Figure 5 shows the TF-XRD patterns of Ti metal soaked in an SBF for 1 day after heat treatment at various temperatures following NaOH and HCl treatments. From Fig. 5, it can be seen that apatite had precipitated on the Ti metal heat-treated at temperatures in the range 500–700°C. These results indicate that the spherical particles observed on the surface of the Ti metal samples in Fig. 4 were composed of apatite.

3.3 Zeta potential of treated Ti metal

Figure 6 shows the zeta potential of the surface of Ti metal subjected to heat treatment at various temperatures

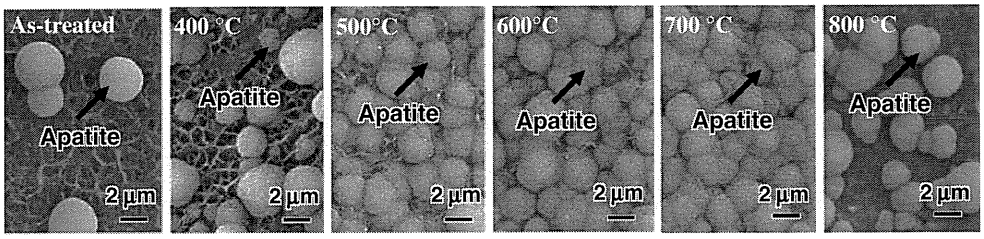

Fig. 4 FE-SEM photographs of surfaces of Ti metals soaked in SBF for 1 day, after heat treatments at various temperatures following the NaOH and HCl treatments

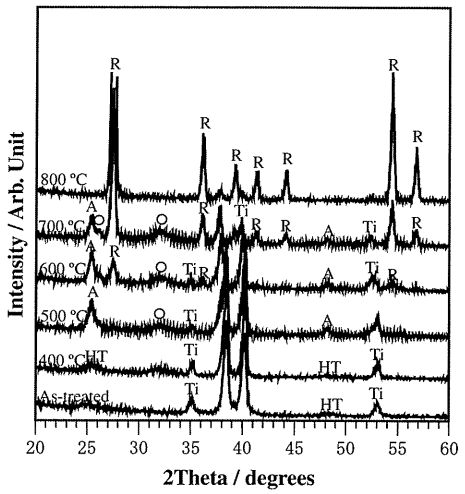

Fig. 5 TF-XRD patterns of the surfaces of Ti metals soaked in SBF for 1 day after heat treatments at various temperatures following the NaOH and HCl treatments. *Ti* α Titanium, *HT* Hydrogen titanate, *A* anatase, *R* Rutile, *O* Apatite

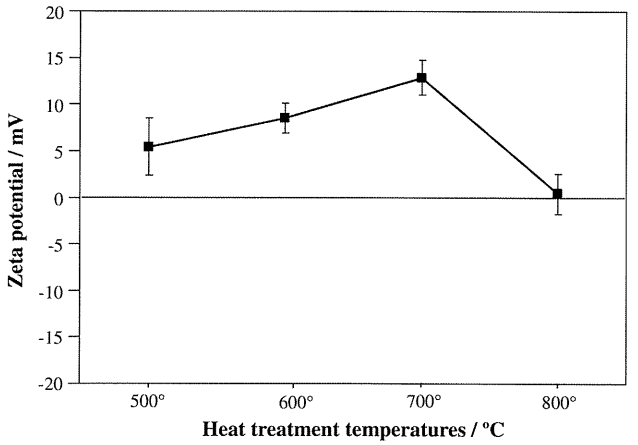

Fig. 6 Zeta potentials of surfaces of Ti metals subjected to heat treatments at various temperatures after NaOH and HCl treatments

following NaOH and HCl treatments. The zeta potential of the samples that had been heat-treated at temperatures below 400°C was not able to be measured, because no, or only a thin, insulating titanium oxide layer had formed on the surface. The Ti metal heat-treated at temperatures in the range 500–700°C exhibited a positive zeta potential that increased with increasing heat treatment temperature up to 700°C, while the Ti metal samples heat-treated at 800°C exhibited a zeta potential of zero.

3.4 XPS spectra of treated Ti metal

Figure 7 shows the XPS spectra of the Ca and P ions on the surface of the Ti metal samples subjected to heat treatment at 400, 600, and 800°C as a function of the soaking time in an SBF after NaOH and HCl treatments. From Fig. 7, it can be seen that Ti metal treated with NaOH and HCl solutions that was subsequently heat-treated at 400°C adsorbed both calcium and phosphate ions almost simultaneously on its surface from the initial stages of soaking in the SBF, whereas Ti metal samples heat-treated at 600 and 800°C only adsorbed phosphate ions during the early stages of soaking in the SBF.

Figure 8 shows the XPS spectra of Cl ions of the surface of Ti metal subjected to heat treatment at 600 and 800°C after NaOH and HCl treatments. From Fig. 8, it can be seen that Cl ions were adsorbed on the surface of the Ti metal after the NaOH and HCl treatments, and that these ions remained on the surface even after the subsequent heat treatment at 600°C, but the samples showed a slight decrease in the number of Cl ions after a heat treatment at 800°C.

4 Discussion

It is apparent from the experimental results described above that the nanometer scale roughness formed on the surface of Ti metal after the NaOH treatment remained after the HCl treatment, and even after a subsequent heat treatment at temperatures below 700°C (see Fig. 1). The decrease in roughness at a heat treatment temperature of 800°C is because of sintering and thickening of the surface oxide layer. The NaOH- and HCl-treated Ti metal formed titanium oxide of anatase and rutile phases when heat-treated at temperatures above 500°C (see Fig. 2).

The scratch resistance of the surface of NaOH- and HCl-treated Ti metal increased with the formation of a titanium oxide layer for heat treatment temperatures above 500°C, but decreased for a heat treatment temperature of 800°C. This decrease may be attributed to the difference in thermal expansion coefficients between the Ti metal substrate and the thick titanium oxide layer.

The titanium oxide formed on the NaOH- and HCl-treated Ti metal samples showed a high apatite-forming ability in an SBF when the temperature of the heat treatment was in the range 500–700°C. This high apatite-forming ability was not attributable to the surface roughness, since the surface roughness of Ti metal samples heat-treated in this temperature range was not different from that of samples heat-treated at lower temperature. Nor was it attributable to a specific crystalline phase, as the ratio of rutile to anatase on the surface of the Ti metal samples was largely changed in this temperature range (see Fig. 2). Therefore, the high apatite-forming ability was attributed to the positive surface charge, as the Ti metal samples only showed a positive zeta potential when the samples were heat-treated in the temperature range of 500–700°C (see Fig. 6). When the Ti metal samples had a positively charged surface,

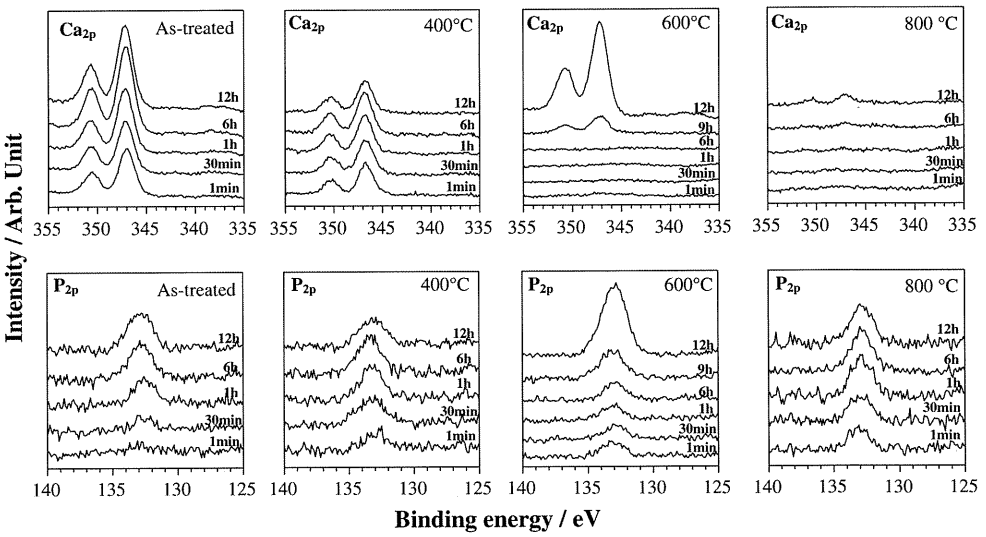

Fig. 7 XPS spectra of Ca and P of the surface of Ti metals as a function of soaking period in SBF subjected to heat treatments at 400, 600 and 800°C after NaOH and HCl treatments

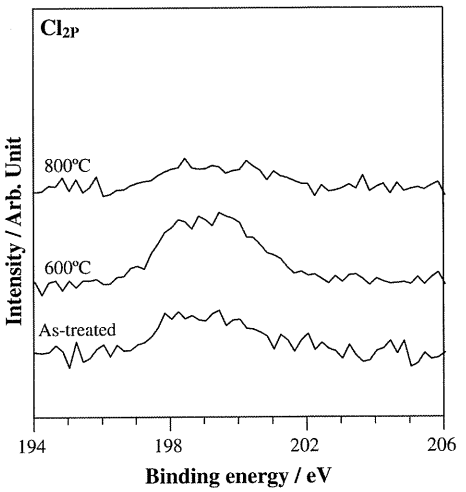

Fig. 8 XPS spectra of Cl ion on the surface of Ti metals as a function of soaking period in SBF subjected to heat treatments at 600 and 800°C after NaOH and HCl treatments

negatively charged phosphate ions were selectively adsorbed on the surface in the SBF. As the phosphate ions begin to accumulate, the surface becomes negatively charged, and, therefore, positively charged calcium ions are adsorbed on the surface to form an apatite layer. This sequential adsorption of phosphate and calcium ions on the Ti metal samples was confirmed by the XPS spectra of Ti metal samples heat-treated at 600°C after NaOH and HCl treatments (see Fig. 7). According to the data in Fig. 7, Ti metal samples heat-treated at 800°C also showed an initial selective adsorption of phosphate ions. However, this tendency was weak. Both Ti metal samples treated with NaOH and HCl solutions and those subsequently heat-treated at 400°C did not show any selective adsorption of phosphate ions, but showed the simultaneous adsorption of calcium and phosphate ions (see Fig. 7). When the calcium and phosphate ions were adsorbed simultaneously on the surface, then its charge was soon neutralized and the calcium phosphate formed could not grow to form an apatite layer.

The reason for the positive surface charge of Ti metal samples heat-treated in the temperature range 500–700°C was attributed to the presence of chloride ions that were adsorbed on the hydrogen titanate layer formed on the Ti metal after the HCl treatment. These remained on the surface, even after the conversion of the hydrogen titanate into titanium oxide by a heat treatment below 700°C. The adsorbed chloride ions dissociate from the surface of the titanium oxide in an SBF to create an acidic environment on the Ti metal. Titanium oxide has been reported to have a positively charged surface in an acidic environment [1]. Above a temperature of 800°C, the chloride ions on the surface of the titanium oxide decompose (see Fig. 8), and so do not form a strong acidic environment and a positive surface charge in an SBF.

Recently, it was reported that Ti metal subjected to a mixed acid treatment shows high apatite-forming ability when it was heat-treated at temperatures ranged from 500 to 650°C, and that their high apatite-forming abilities are also attributed to their positive surface charge [15]. This is consistent with the present results.

It has been reported that osteoconduction and osteoinduction are closely related to an apatite-forming ability [16]. Our present results could establish the fundamental conditions required for chemical and heat treatments to obtain porous titanium metal that could induce high osteoconductivity and osteoinductivity.

5 Conclusions

1. A nanometer scale roughness formed on Ti metal samples after an NaOH treatment remains after an HCl

treatment and a subsequent heat treatment below 700°C.

2. NaOH- and HCl-treated Ti metal forms titanium oxide of anatase and rutile phases on its surface after a heat treatment above 500°C.
3. The scratch resistance of the surface of Ti metal increases with the formation of titanium oxide up to 700°C, and then decreases with increasing temperature.
4. The apatite-forming ability in an SBF of Ti metal is remarkably high when the Ti metal is heat-treated in the temperature range 500–700°C after NaOH and HCl treatments.
5. The high apatite-forming ability of Ti metal subjected to the above treatments is attributed to positive surface charges.
6. These positive surface charges arise from the presence of chloride ions adsorbed on the titanium oxide layer, which dissociate in an SBF to give an acidic environment.
7. Our present results could establish the conditions required for the chemical and heat treatments to obtain porous Ti metal oxide that could induce high osteoconductivity and osteoinductivity.

References

1. Textor M, Sittig C, Frauchiger V, Tosatti S, Brunette DM. Properties and biological significance of natural oxide films on titanium and its alloys. In: Brunette DM, Tengvall P, Textor M, Thomsen P, editors. Titanium in medicine. Germany: Springer; 2001. p. 171–230.
2. Hacking SA, Tanzer M, Harvey EJ, Krygier JJ, Bobyn JD. Relative contributions of chemistry and topography to the osseointegration of hydroxyapatite coatings. Clin Orthop Relat Res. 2002;405:24–38.
3. Kokubo T, Miyaji F, Kim HM, Nakamura T. Spontaneous formation of bonelike apatite layer on chemically treated titanium metals. J Am Ceram Soc. 1996;79:1127–9.
4. Kim HM, Miyaji F, Kokubo T, Nakamura T. Preparation of bioactive Ti and its alloy via simple chemical surface treatment. J Biomed Mater Res. 1996;32:409–17.
5. Yan WQ, Nakamura T, Kobayashi M, Kim HM, Miyaji F, Kokubo T. Bonding of chemically treated titanium implants to bone. J Biomed Mater Res. 1997;37:267–75.
6. Nishiguchi S, Fujibayashi S, Kim HM, Kokubo T, Nakamura T. Biology of alkali- and heat-treated titanium implants. J Biomed Mater Res. 2003;67A:26–35.
7. Kawanabe K, Ise K, Goto K, Akiyama H, Nakamura T, Kaneuji A, Sugimori T, Matsumoto T. A new cementless total hip arthoplasty with bioactive titanium porous-coating by alkaline and heat treatment: average 4.8-year results. J Biomed Mater Res. 2009;90B:476–81.
8. Pattanayak DK, Kawai T, Matsushita T, Takadama H, Kokubo T, Nakamura T. Effect of HCl concentrations on apatite-forming ability of NaOH-HCl- and heat-treated titanium metal. J Mater Sci Mater Med. 2009;20:2401–11.
9. Takemoto M, Fujibayashi S, Neo M, Suzuki J, Kokubo T, Nakamura T. Mechanical properties and osteoconductivity of porous bioactive titanium. Biomaterials. 2005;26:6014–23.
10. Takemoto M, Fujibayashi S, Neo M, Suzuki J, Matsushita T, Kokubo T, Nakamura T. Osteoinductive porous titanium implants: effect of sodium removal by dilute HCl treatment. Biomaterials. 2006;27:2682–91.
11. Takemoto M, Fujibayashi S, Neo M, So K, Akiyama N, Matsushita T, Kokubo T, Nakamura T. A porous bioactive titanium implant for spinal interbody fusion: an experimental study using a canine model. J Neurosurg Spine. 2007;7:435–43.
12. Kokubo T, Takadama H. How useful is SBF in predicting in vivo bone bioactivity? Biomaterials. 2006;27:2907–15.
13. Sun X, Li Y. Synthesis and characterization of ion-exchangeable titanate nanotubes. Chem Eur J. 2003;9:2229–38.
14. Tsai CC, Teng H. Structural features of nanotubes synthesized from NaOH treatment on TiO_2 with different post-treatments. Chem Mater. 2006;18:367–73.
15. Kokubo T, Pattanayak DK, Yamaguchi S, Takadama H, Matsushita T, Kawai T, Takemoto M, Fujibayashi S, Nakamura T. Positively charged bioactive titanium metal prepared by simple chemical and heat treatments. J R Soc Interface. 2010;7:S503–13.
16. Bruijn JDD, Shankar K, Yuan H, Habibovic P. Osteoinduction and its evaluation. In: Kokubo T, editor. Bioceramics and their clinical applications. Cambridge: Woodhead publishing Ltd; 2008. p. 199–219.

JOURNAL OF THE ROYAL SOCIETY Interface

Positively charged bioactive Ti metal prepared by simple chemical and heat treatments

Tadashi Kokubo, Deepak K. Pattanayak, Seiji Yamaguchi, Hiroaki Takadama, Tomiharu Matsushita, Toshiyuki Kawai, Mitsuru Takemoto, Shunsuke Fujibayashi and Takashi Nakamura

J. R. Soc. Interface 2010 **7**, S503-S513 first published online 5 May 2010
doi: 10.1098/rsif.2010.0129.focus